of the detailed Coulomb trajectories are required. Hence, the validity of scaling the D^+-D collision[2] depends strongly upon $Z/M_r = 1.00$ for velocities near the threshold. Collision systems where $Z/M_r = 0.91$ (i.e., $^{22}Ne^+$-^{22}Ne) can lead to variations of K vacancy yields as high as 40%. At higher relative velocities, however, the relative velocity scaling does appear to be valid for collision systems with $Z/M_r \approx 1$ as predicted.[2]

Since we completed these experiments, Taulbjerg and Macek[3] have kindly provided explicit calculation of the isotope effects we observed for the collision system used in our experiment, based on a mass-dependent refinement of their original papers[2] to be published in the very near future.[9,10] The solid curves in Fig. 1 display the results of their mass-dependent treatment, excellently accounting for the large isotope effects seen in our experiments. The new mass-dependent treatment of vacancy production in assymmetric collisions by Taulbjerg, Briggs, and Vaaben[9] has thereby been shown to be excellent. The demonstrated size of such isotope effects even in total crosssection measurements provides a promising experimental tool for use in studying other collision systems.

We acknowledge stimulating discussions with J. H. Macek, W. Brandt, and J. S. Briggs concerning these experiments.

*Work supported in part by the U. S. Office of Naval Research, the National Science Foundation, and the U. S. Energy Research and Development Administration.

[1]W. Lichten, Phys. Rev. 164, 131 (1967).

[2]J. S. Briggs and J. Macek, J. Phys. B 5, 579 (1972).

[3]K. Taulbjerg and J. H. Macek, private communication.

[4]F. W. Saris and D. Onderdelinden, Physica (Utrecht) 49, 441 (1970).

[5]K. H. Schartner, H. Schafer, and R. Hippler, Phys. Lett. 46A, 31 (1973).

[6]N. Stolterfoht, D. Schneider, D. Burch, B. Aagaard, E. Bøving, and B. Fastrup, Phys. Rev. A 12, 1313 (1975).

[7]J. S. Briggs, in *Proccedings of the International Conference on Inner-Shell Ionization Phenomena and Future Applications, Atlanta, Georgia, 1972,* edited by R. W. Fink, S. T. Manson, J. M. Palms, and P. V. Rao, CONF-720 404 (U. S. Atomic Energy Commission, Oak Ridge, Tenn., 1973), Vol. 2, p. 1209.

[8]B. Fastrup, G. Hermann, and O. C. Kessel, Phys. Rev. Lett. 27, 771 (1971).

[9]K. Taulbjerg, J. S. Briggs, and J. Vaaben, to be published.

[10]K. Taulbjerg, in Proceedings of the Second International Conference on Inner-Shell Ionization Phenomena, Freiburg, Germany, 29 March–2 April 1976 (to be published).

Angular Distributions of Electrons from Resonant Two-Photon Ionization of Sodium

J. A. Duncanson, Jr., M. P. Strand, A. Lindgård, and R. S. Berry

Department of Chemistry, The University of Chicago, Chicago, Illinois 60637

(Received 13 July 1976)

Sodium atoms are excited to either the $3^2P_{1/2}$ or $3^2P_{3/2}$ state using a linearly polarized dye-laser beam and are subsequently ionized using a linearly polarized nitrogen-laser beam. Angular distributions of the ejected electron have been both measured and calculated for several relative orientations of the photon polarization vectors. The difference between the s- and d-continuum partial-wave phase shifts $\delta_s - \delta_d$ and the ratio of the radial dipole matrix elements (d_s/d_d) are obtained.

We report the first measurement of anisotropic angular distributions of electrons from resonant two-photon ionization of atoms. An isotropic ensemble of sodium atoms in their $3^2S_{1/2}$ ground state is excited to either the $3^2P_{1/2}$ or the $3^2P_{3/2}$ level by a linearly polarized beam from a tunable dye laser, producing an aligned intermediate state. After a 5-nsec delay, they are ionized by a linearly polarized nitrogen laser beam of wavelength 337.1 nm. For the two-step ionization process, the intensity of electrons ejected in direction $\hat{\Omega}$ is given by

$$\frac{d\sigma}{d\Omega} = \text{const} \sum_{\substack{\Lambda_1\Lambda_2 \\ LM}} Y_{LM}(\hat{\Omega})(\rho_{\Lambda_1}{}^{(1)}\rho_{\Lambda_2}{}^{(2)})_{LM} C(\Lambda_1, \Lambda_2, L), \tag{1}$$

where

$$C(\Lambda_1,\Lambda_2,L)=\sum_{ll'}\begin{Bmatrix}1 & 1 & \frac{1}{2}\\ j & j & \Lambda_1\end{Bmatrix}^2\begin{pmatrix}1 & 1 & \Lambda_1\\ 1 & 1 & \Lambda_2\\ l & l' & L\end{pmatrix}\langle L0|l0,l'0\rangle\left[\frac{(2\Lambda_1+1)(2\Lambda_2+1)(2l+1)(2l'+1)}{4\pi(2L+1)}\right]^{1/2}$$

$$\times d_l d_{l'}\cos(\delta_l-\delta_{l'})[\max(l,1)\max(l',1)]^{1/2}(-1)^{\max(l,1)}(-1)^{\max(l',1)},$$

the d_l's are the radial dipole matrix elements from the intermediate $3P_j$ state to the continuum S and D states, and the δ_l's are the non-Coulomb phase shifts of those continuum states. $(\rho_{\Lambda_1}{}^{(1)}\rho_{\Lambda_2}{}^{(2)})_{LM}$ is the polarization density matrix of the combined two-photon system expressed in irreducible tensorial components. Λ_1 and Λ_2 take on the values 0 and 2, while L takes on the values 0, 2, and 4.

Figure 1 defines the geometry of the system. The electron trajectory is described by the polar angles θ and φ. The axis of polarization of the second photon defines the positive z axis. The polarization axis of the first photon lies in the x-z plane at an angle η with respect to this z axis. The laser beams propagate along the y axis. With this geometry, the cross section may be expressed as

$$\frac{d\sigma}{d\Omega}=\text{const}\sum_l\sum_{M=0}^{L}\alpha_{LM}P_L{}^M(\cos\theta)\cos(M\varphi), \tag{2}$$

where $P_L{}^M(\cos\theta)$ are the normalized associated Legendre polynomials and

$$\alpha_{LM}=(2-\delta_{M,0})(2\pi)^{-1/2}(-1)^M\sum_{\Lambda_1\Lambda_2}(\rho_{\Lambda_1}{}^{(1)}\rho_{\Lambda_2}{}^{(2)})_{LM}C(\Lambda_1,\Lambda_2,L). \tag{3}$$

The α_{LM} depend on η through $\rho_{\Lambda_1}{}^{(1)}$. When the intermediate state is $3\,^2P_{3/2}$, there are in general seven nonzero α_{LM} in Eq. (2) corresponding to $(L,M)=(0,0)$, $(2,0)$, $(2,1)$, $(2,2)$, $(4,0)$, $(4,1)$, and $(4,2)$. The presence of the $(2,1)$ and $(4,1)$ terms introduce $\sin2\theta$ and $\sin4\theta$ terms into the angular distribution. For $\eta=90°$, the two sine terms drop out; and for $\eta=0°$, only the terms $(L,M)=(0,0)$, $(2,0)$, and $(4,0)$ appear in (2).

When the intermediate state is $3\,^2P_{1/2}$, the $\Lambda_1=2$ terms do not contribute, the angular distribution is independent of the (linear) polarization direction of the first photon, and the distribution reduces to the one-photon formula

$$\frac{d\sigma}{d\Omega}=\frac{\sigma_{\text{tot}}}{4\pi}[1+\beta P_2(\cos\theta)].$$

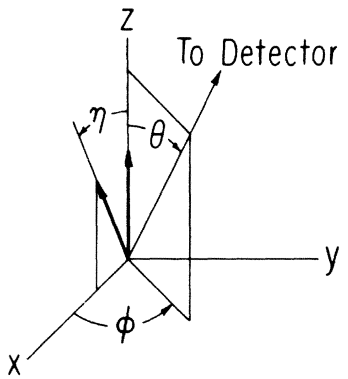

FIG. 1. System geometry. The electron trajectory is defined by θ and φ. The second photon polarization axis defines the z axis. The axis of the first photon polarization lies in the x-z plane at an angle η from the z axis.

The measurements were made by intersecting a sodium beam with two linearly polarized, nearly collinear laser beams, one from a nitrogen laser, the second from a dye laser pumped by half of the nitrogen-laser beam.[1] The polarization directions were rotated between laser pulses through 18° intervals (always at a fixed angle η between them), with the detector fixed to provide rapid sampling of the angular distribution. The photoelectrons were accelerated, detected by a Channeltron, and counted.

The intermediate state was not optically saturated. Photoelectron intensity was proportional to the product of the dye-laser and the N_2-laser intensities over a range of two orders of magnitude. The peak of the nitrogen-laser pulse [10 nsec full width at half-maximum (FWHM)] arrived 5 nsec after the peak of the dye-laser pulse (4 nsec FWHM) insuring a stepwise two-photon ionization.

Examples of our experimental results are shown in Fig. 2, for $3\,^2P_{1/2}$, and in Fig. 3, for $3\,^3P_{3/2}$. In Fig. 2, the dotted curve is a least-squares fit by an equation of the form

$$W(\theta)=a_0+a_1\cos^2\theta, \tag{4}$$

normalized to 1 at 0°. The coefficients obtained were $a_0=0.041\pm0.02$, $a_1=0.959\pm0.02$, and $\beta=(1$

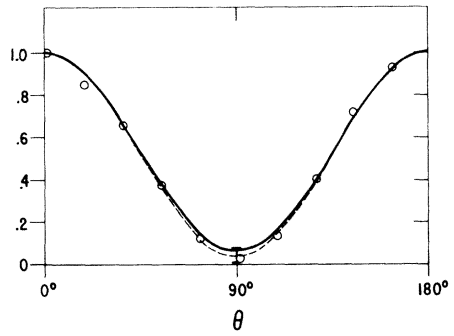

FIG. 2. Experimental measurement on $3\,^2P_{1/2}$ level of sodium. Circles, experimental points; dashed line, least-squares fit; solid line, theoretical curve. Both curves are normalized to 1 at 0°.

$-a_0)/(a_0+\frac{1}{2}) = 1.77 \pm 0.10$. Theoretical values, obtained by the process described below, are $a_0 = 0.062\,50$, $a_1 = 0.937\,50$, and $\beta = 1.667$, consistent with the experimental values. A fit by Eq. (4) with a $\cos^4\theta$ term added showed the $\cos^4\theta$ term to be zero within the experimental error.

Figure 3 shows experimental and calculated angular distributions taken through the $3\,^2P_{3/2}$ level.

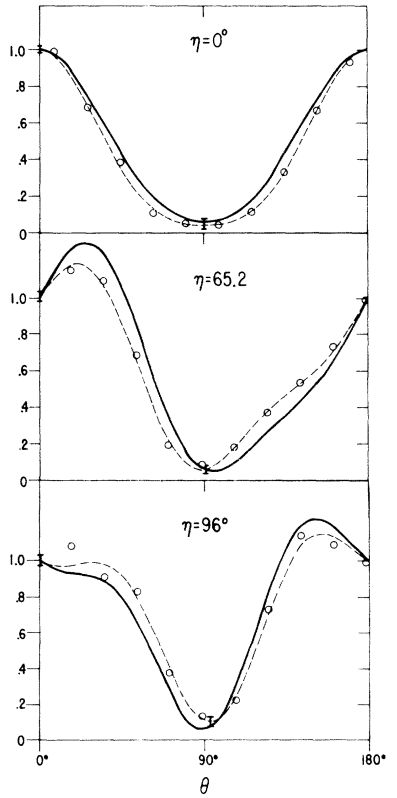

FIG. 3. Experimental measurements on $3\,^2P_{3/2}$ level of sodium, for $\varphi = 0°$. Circles, experimental points; dashed lines, least squares fit; solid lines, theoretical curves. All curves normalized to 1 at 0°.

Since the detector lies in the X-Z plane of Fig. 1, $\varphi = 0°$ and (2) reduces to the form

$$W(\theta) = c_1 + c_2\cos 2\theta + c_3 \sin 2\theta + c_4 \cos 4\theta + c_5 \sin 4\theta. \quad (5)$$

Least-squares fits of the data with (5) are shown as dashed curves in Fig. 3; the solid curves are calculated angular distributions, using best-fitting microscopic parameters. All curves are normalized to 1 at 0°. Table I lists the experimental coefficients. The experimental angular distributions clearly show the distinctive features of two-photon ionization. The $\cos 4\theta$ term is evident in all cases, and terms in $\sin 2\theta$ and $\sin 4\theta$ are required to account for the asymmetry in the cases $\eta = 65°$ and $\eta = 96°$. Note also that the sine terms, with the coefficients c_3 and c_5, are zero to within 0.1 standard deviation for $\eta = 0°$.

The general theoretical formula (2) contains seven α_{LM} coefficients, while our distributions are described by (5), which contains four independent coefficients because we made measurements only for $\varphi = 0$ and normalized the coefficients to 1 at $\theta = 0°$. However, these normalized values retain all the dynamical information, the ratio of the radial dipole matrix elements d_0/d_2, and the partial-wave phase-shift term $\cos(\delta_0 - \delta_2)$.

Starting with an initial theoretical estimate[2] of the matrix-element ratio $d_0/d_2 = 1.3$ and picking the arbitrary choice of $\cos(\delta_0 - \delta_2) = 1$, we obtained first-trial angular distributions which agree reasonably well qualitatively with the experiment, but they show some quantitative differences. The matrix-element ratio was then varied from +100 through 0 to −100, which produced

TABLE I. Experimental normalized least-squares-fit coefficients (1-standard-deviation error range listed under each value).

η	c_1	c_2	c_3	c_4	c_5
0°	0.432	0.481	0.0012	0.087	0.0005
	(0.008)	(0.012)	(0.011)	(0.010)	(0.011)
65.2°	0.596	0.470	0.193	−0.066	0.118
	(0.012)	(0.014)	(0.018)	(0.017)	(0.015)
96°	0.743	0.447	−0.015	−0.190	−0.070
	(0.016)	(0.021)	(0.025)[a]	(0.020)	(0.021)[a]

[a]Because this value of η is very close to 90° where the $\sin 2n\theta$ terms are zero, the values of c_3 and c_5 are changing rapidly. Duplicate experiments indicate that their values are not reproducible to within 1 standard deviation.

variations in the qualitative shapes of the angular distributions, marked enough that we were confident, even from a visual inspection, that the initial choice for the parameters was nearly correct. The final evaluation of experimental values of the two dynamical parameters from the angular-distribution coefficients was carried out by searching the two-dimensional space of these parameter values to obtain a region of reasonably good fit between the experimental and calculated distributions, and then finding a best fit within the region. The parameters must be the same for all η. We also assumed they are the same for the $3\,^2P_{1/2}$ and $3\,^2P_{3/2}$ levels because the spin-orbit coupling is small. These constraints assure that there is sufficient experimental data to overdetermine the dynamical parameters. The parameter range which gave a reasonable fit is $d_0/d_2 = 1.6$ to 2.3 and $\cos(\delta_0 - \delta_2) = 0.8$ to 1.0. The best fit was at $d_0/d_2 = 2.0$ and $\cos(\delta_0 - \delta_2) = 1.0$. The corresponding best-fit values of c_n are listed in Table II.

TABLE II. Theoretical normalized c_n coefficients, using the best-fit values of the two dynamical parameters $\sigma_0/\sigma_2 = 2.0$ and $\cos(\delta_0 - \delta_2) = 1.0$ and normalized such that the value of the angular distribution at $\theta = 0°$, $\varphi = 0°$ is 1.

η	c_1	c_2	c_3	c_4	c_5
0°	0.4785	0.4688	0	0.0527	0
65.2°	0.6207	0.4688	0.3505	−0.0895	0.1051
96°	0.7310	0.4688	−0.1416	−0.1998	−0.0425

[1]T. W. Hänsch, Appl. Opt. 11, 895 (1972).
[2]A. Burgess and M. J. Seaton, Mon. Not. Roy. Astron. Soc. 120, 121 (1960).

Spontaneous Raman Processes in Multiphoton Excitation of Sodium*

P. B. Hogan, J. L. Carlsten, F. M. J. Pichanick,† S. J. Smith, and W. W. Smith‡
Joint Institute for Laboratory Astrophysics, University of Colorado and National Bureau of Standards, Boulder, Colorado 80309
(Received 15 June 1976)

We have observed spontaneous Raman processes in a sodium atomic beam. When one sodium $3p\,^2P$ fine-structure level is strongly excited by a dye laser, the other level, is weakly populated by spontaneous Raman emission and the absorption of another laser photon. This effect is detected by further stepwise excitation plus photoionization. The observed magnitude agrees well with theory. This technique is much more sensitive than methods involving direct observation of the Raman emission.

We have extended the recent multiphoton-ionization studies by Lambropoulos *et al.*[1] and have observed *spontaneous* Raman process in an atomic beam of sodium. Nearly all previous experiments on Raman processes in atomic systems have involved the observation of *stimulated* emission,[2] although spontaneous emission has been observed in a dense cell of thallium.[3] Combinations of laser intensities and atomic densities in the previous experiments were many orders of magnitude larger than those in the present work, which uses tunable dye lasers and an atomic beam. Under those conditions, the intensity of Stokes or anti-Stokes radiation is much too small to be observed directly.

The main features of our apparatus have been described previously. Coincident light beams from synchronized, flashlamp-pumped yellow and blue dye lasers interacted at right angles with a sodium atomic beam. The density of the atomic beam was about 10^{10} atoms/cm^3; and the power densities of the yellow and blue lasers were approximately 0.5 and 0.05 MW/cm^2, respectively. After each laser pulse, the photoions were collected and accelerated into an electron-multiplier detector by means of a suitably delayed, pulsed electric field.

Figure 1 illustrates the two complementary Raman processes which are involved in our experiments. In Fig. 1(a), the $3p\,^2P_{1/2}$ level is populated by resonance excitation from the $3s\,^2S_{1/2}$ ground state with a yellow dye laser. In the presence of the strong field of the yellow laser, there is a probability of spontaneous decay from the $3p\,^2P_{1/2}$ to a virtual level (shown as a broken line) which can be excited in resonance to the $3p\,^2P_{3/2}$ level by absorption of a second photon from the yellow laser. The $3p\,^2P_{3/2}$ is thus weakly populated in the field of a laser tuned to saturate the $3s\,^2S_{1/2} \rightarrow 3p\,^2P_{1/2}$ transition. The photon emitted